

The influence of the focusing effect on the x-ray absorption fine structure above all the tungsten L edges in non-stoichiometric tungsten oxides

A Kuzmin and J Purans

Institute of Solid State Physics, University of Latvia, Kengaraga 8, LV-1063 Riga, Latvia

Received 2 August 1993, in final form 23 September 1993

Abstract. The role of multiple-scattering contributions in the formation of the x-ray absorption fine structure (XAFS) above tungsten L edges is discussed for the non-stoichiometric tungsten oxides WO_{3-x} . It is found that the presence of linear or near-linear atomic chains in the WO_{3-x} crystal structure leads, due to the focusing effect, to a strong increase in the XAFS amplitude, which results in an admixture of the L_2 -edge XAFS with the XAFS above the L_1 edge.

1. Introduction

It is well known that multiple-scattering (MS) signals contribute, often significantly, to x-ray absorption fine structure (XAFS), especially when linear or near-linear atomic chains exist in the studied compound. Two such contributions are most important in the XAFS spectra of metal oxides (MeO_x) with a perovskite-type structure measured above the metal absorption edge [1]: (i) the MS signals in the first coordination shell, generated within $O-Me_a-O$ chains (where Me_a is the absorber), which contribute mainly at the beginning of the XAFS spectrum, and (ii) the MS signals in the second coordination shell, generated within Me_a-O-Me chains, which contribute mainly in the high-energy range. The reason why these two MS signals are more intense than others is the particular role played by the intermediate atom (Me_a in the first case and O in the second case), which significantly increases the amplitude of the photoelectron wave in the forward-scattering process. This phenomenon is called the 'focusing' effect. To illustrate it, the angular dependence of the atomic scattering amplitude is shown in figure 1 for oxygen and tungsten atoms, forming compounds considered in this work.

The scattering amplitude for each atom was calculated using the standard approach to the scattering process of a spherical photoelectron wave by a spherically symmetric atomic potential [2]:

$$f(k, R, \theta) = \frac{1}{k} \sum_{\bar{l}} (2\bar{l} + 1) t_{\bar{l}} P_{\bar{l}}(\cos \theta) \sum_{\bar{l}} (2\bar{l} + 1) \left[\begin{pmatrix} \bar{l} & \bar{l} & \bar{l} \\ 0 & 0 & 0 \end{pmatrix} C_{\bar{l}}(kR) \right]^2 \quad (1)$$

where R is the curvature radius of the photoelectron wave, θ is the scattering angle ($\theta=0^\circ$ for the back-scattering process and $\theta=180^\circ$ for the forward-scattering process), l is the angular momentum of the photoelectron, t_l is the scattering T -matrix element defined by $t_l = e^{i\phi_l} \sin(\delta_l)$, where δ_l are the partial phase shifts calculated from the radial part of the Schrödinger-like equation [3], and $C_l(kR)$ is the polynomial factor introduced by Rehr and

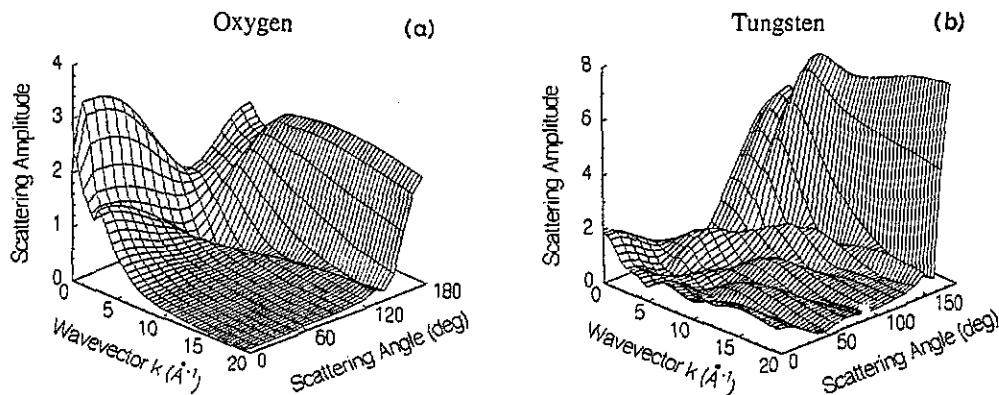


Figure 1. The angular dependence of the atomic scattering amplitude for oxygen and tungsten atoms. The angle $\theta = 0^\circ$ corresponds to the back-scattering process and $\theta = 180^\circ$ to the forward-scattering process.

co-workers [2]. The value of R was chosen to be equal to 1.9 \AA for oxygen and 3.8 \AA for tungsten. Both values are close to the typical W–O and W–W distances in WO_{3-x} crystals. The origin of the focusing effect is obvious from the large difference, particularly at high energies, between the back- and forward-scattering amplitudes, which is clearly visible in figure 1. It is also clear from the behaviour of the amplitudes why the MS signals generated within two atomic chains O–W_a–O and W_a–O–W mainly contribute in different energy ranges of XAFS (at low and high energies, respectively). The reason is that the XAFS amplitude depends on the product of atomic scattering amplitudes of all atoms participating in the scattering process. For example, for the O–W_a–O chain and the W_a → O → W_a → O → W_a MS path with $\widehat{\text{OW}_a\text{O}} = 180^\circ$, the XAFS amplitude is proportional to two back-scattering amplitudes of oxygen and one forward-scattering amplitude of tungsten; the product decreases when the energy increases. On the other hand, for the W_a–O–W chain and the W_a → O → W → O → W_a MS path with $\widehat{\text{W}_a\text{OW}} = 180^\circ$, the result of the product of two forward-scattering amplitudes of oxygen and the back-scattering amplitude of tungsten leads to an increase of the total amplitude at high energies.

In addition to the MS contributions, the amplitude of the XAFS signal at high energies is also affected by an exponential damping term of type $\exp(-2\sigma^2k^2)$, describing both thermal and static disorder [4]. Competition between the variation of the $\widehat{\text{MeOMe}}$ angle and the degree of disorder leads for Me–O–Me chains to large changes in the XAFS signal amplitude in the high-energy region, which can result in some interesting phenomena. In particular, the effect of the L_1 and L_2 XAFS mixing was pointed out by us recently for ReO_3 [1]. (A similar effect was found earlier for L edges of gold [5].) It was shown that the strong MS contribution from the Re–O–Re linear chains leads to a significant decrease of the amplitude damping with the increase of the photoelectron energy. As a result, due to the small separation of rhenium L_1 and L_2 edges ($\Delta E_{L_1-L_2} \simeq 568 \text{ eV}$), the fine structure above the L_1 edge is a superposition of two XAFS signals from L_1 and L_2 edges, with a very significant contribution of the latter [1].

In WO_{3-x} compounds, the correlation between the amplitude of the W L_3 -edge XAFS signal and the W L_1 -edge XANES (x-ray absorption near-edge structure) was pointed out earlier [6], and it was suggested that the origin of some features in the W L_1 -edge XANES is connected with the focusing effect in the second coordination shell. In this paper we present

a detailed interpretation of the W L_1 -edge fine structure and show that in non-stoichiometric tungsten oxides the same effect of the L_2 - and L_1 -edge XAFS mixing as in ReO_3 occurs.

2. Results and discussion

X-ray absorption spectra of tungsten L edges in finely ground WO_{3-x} polycrystals were recorded in transmission mode at room temperature at the ADONE storage ring on the BX-1 PWA beam line using synchrotron radiation from a wiggler source. The experimental details and the partial analysis of experimental data were published previously [7, 8]. Note that for tungsten the separation between the L_2 and L_1 edges (see figure 2) is even smaller ($\Delta E_{L_1-L_2} \simeq 556$ eV) compared to rhenium.

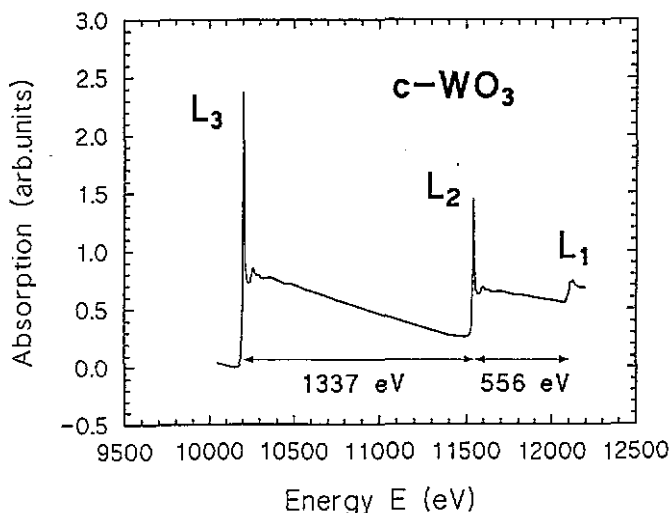


Figure 2. The x-ray absorption spectrum of tungsten in WO_3 . Note that the separation of tungsten L_2 and L_1 edges is less than half that of the L_3 and L_2 edges due to the fact that an overlap of the L_2 -edge fine structure with that above the L_1 edge takes place.

The tungsten L_3 -edge XAFS spectra $\chi(k)k^2$ and their Fourier transforms (FT) are shown in figure 3. There are four groups of peaks in the FT, which are due to (i) the single-scattering (SS) signals from the first shell formed by oxygen atoms, (ii) the MS signals, generated within the first shell, (iii) the SS and MS contributions from the second shell, formed by tungsten atoms, plus the SS and MS contributions from oxygen atoms, and (iv) the signals from the shells beyond the third shell. The structure of WO_{3-x} is based on distorted octahedral WO_6 coordination groups with a wide range of W-O bond lengths (typically, $1.6 < R_{W-O} < 2.4$ Å). The WO_6 octahedra are joined by apexes with $\overline{WOW} > 150^\circ$, and there is also sharing of their edges in the ab plane for $x > 0$. The drastic changes of the amplitude of the second-shell peak, located between 3.2 Å and 4.2 Å, are clearly visible in figure 3(b). Notice that the increase of the second-shell peak amplitude in the FT corresponds to the increase of the XAFS signal at high energies. Such changes of the XAFS amplitude can be attributed to a variation of the values of the \overline{WOW} angles.

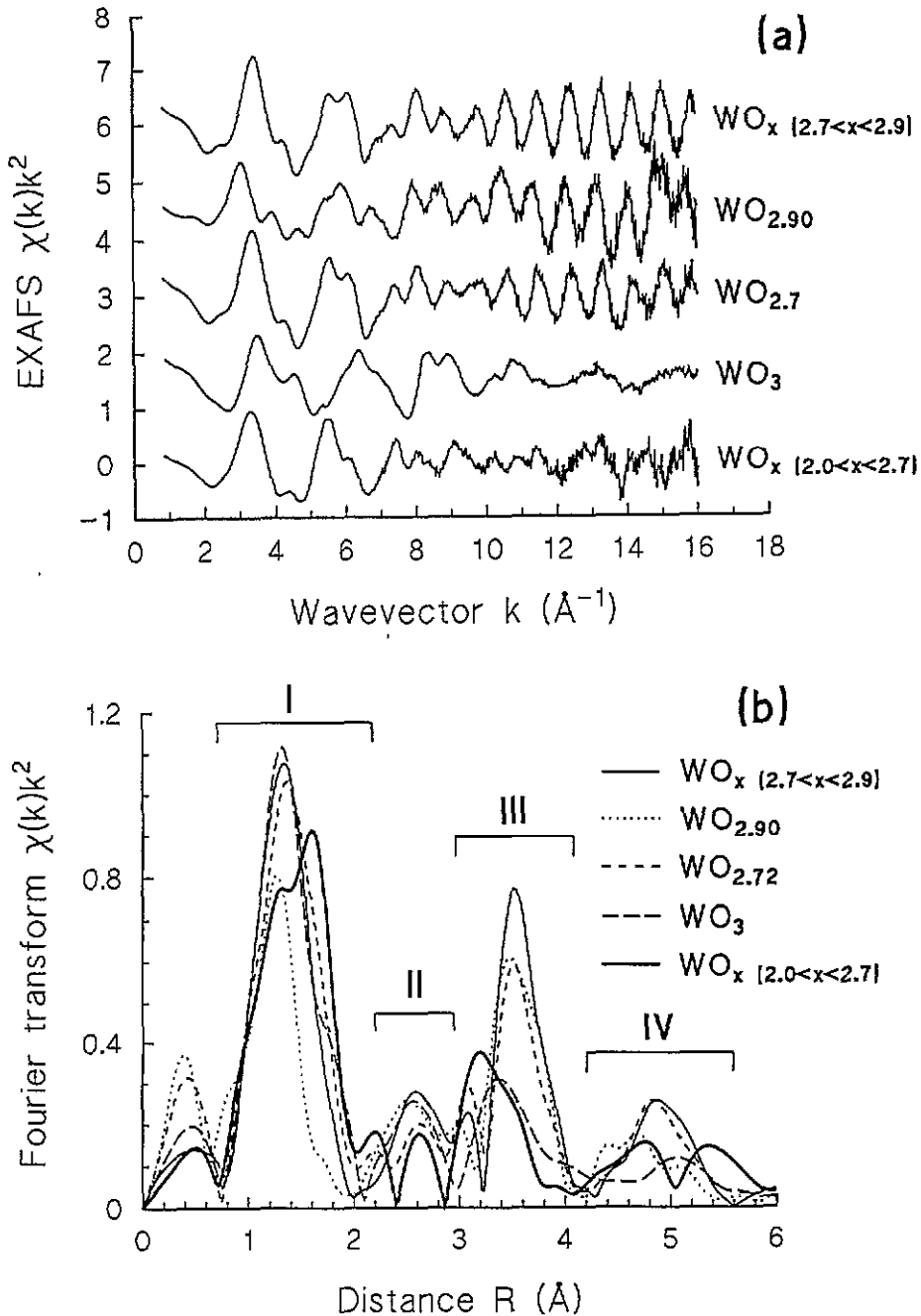


Figure 3. (a) The experimental XAFS $\chi(k)k^2$ spectra of the W L_3 edge in WO_{3-x} . The presence in non-stoichiometric tungsten oxides of near-linear atomic chains leads, due to the focusing effect, to an increase of the signal amplitude at high k -values. (b) Fourier transforms of spectra shown in (a). The four marked ranges are explained in the text.

In stoichiometric WO_3 , the WOW angles along all axes are equal to $\sim 158^\circ$ [9]. In

non-stoichiometric tungsten oxides, the WOW angles are between 150° and 170° , but they are close to 180° in the direction of the c axis [6, 7]. The presence of nearly linear W–O–W atomic chains along the c axis in non-stoichiometric WO_{3-x} leads to strong multiple-scattering in this direction [7], and is the reason why the amplitude of XAFS at high energies increases, while it decreases in stoichiometric WO_3 (figure 3(a)).

The L_1 -edge XANES spectra of WO_{3-x} and ReO_3 , for comparison, are shown in figure 4. The four features A, B, C and D are clearly visible and can be described within the framework of (i) electron transitions and (ii) MS resonances.

The interpretation of electron transitions near the absorption edge will be made using the following notation: the transition from the core atomic state nl into the final state $\overline{n', \epsilon'}$ in the continuum (ϵ) with $n'l'$ atomic character will be denoted as $nl \rightarrow \overline{n', \epsilon'}$ where the bar over $\overline{n', \epsilon'}$ indicates that the final state of the electron is the relaxed excited state in the presence of the core hole at the nl level screened by other electrons. The pre-edge A corresponds to $2s(W) \rightarrow \overline{5, \epsilon d(W)} + \overline{2, \epsilon p(O)}$ transition, which is forbidden in the dipole approximation for a perfect WO_6 octahedron, but becomes allowed when the inversion centre is absent [6, 8]. Its amplitude depends on the degree of WO_6 octahedra distortion, and $2p(O)$ – $5d(W)$ orbital mixing. The pre-edge A has the largest amplitude in stoichiometric tungsten trioxide WO_3 and decreases along the series $WO_{2.90}$, $WO_{x(2.7 < x < 2.9)}$, $WO_{2.7}$, $WO_{x(2.0 < x < 2.7)}$. Such variation is connected with (i) the lowering of the tungsten valence state, which leads to a symmetrization of WO_6 octahedra, and (ii) the increase of the average tungsten–oxygen distance from 1.78 \AA to 1.95 \AA [8]. The second feature B, properly the edge, is assigned to the $2s(W) \rightarrow \overline{6, \epsilon p(W)} + \overline{2, \epsilon p(O)}$ allowed transition.

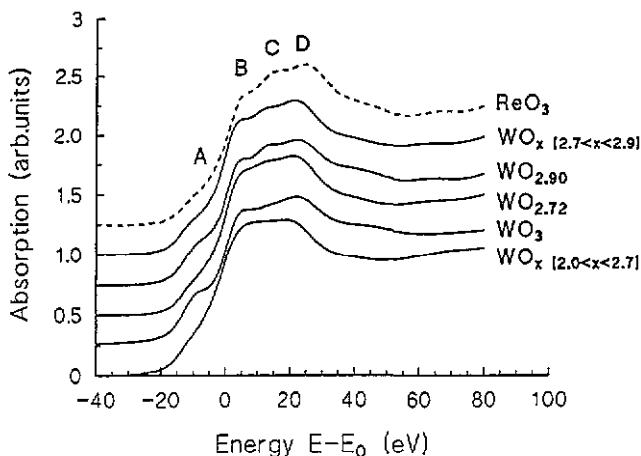


Figure 4. The XANES spectra of the tungsten L_1 edge in WO_{3-x} . The rhenium L_1 -edge XANES spectrum for ReO_3 is also shown for comparison. The origin of the labelled features is discussed in the text.

In the MS approach the first feature A corresponds to poles of the scattering path operator at negative energies, i.e. below the continuum threshold [10]. The origin of other features becomes clear from figure 5 where L_1 - and L_3 -edge XAFS are shown in comparison with the contributions to L_3 -edge XAFS from the four ranges in the FT noted before. In the first approximation, the difference between L_1 - and L_3 -edge XAFS originates from the π factor and a difference in central-atom phase shifts [1]. Therefore, the experimental L_1 -edge signal

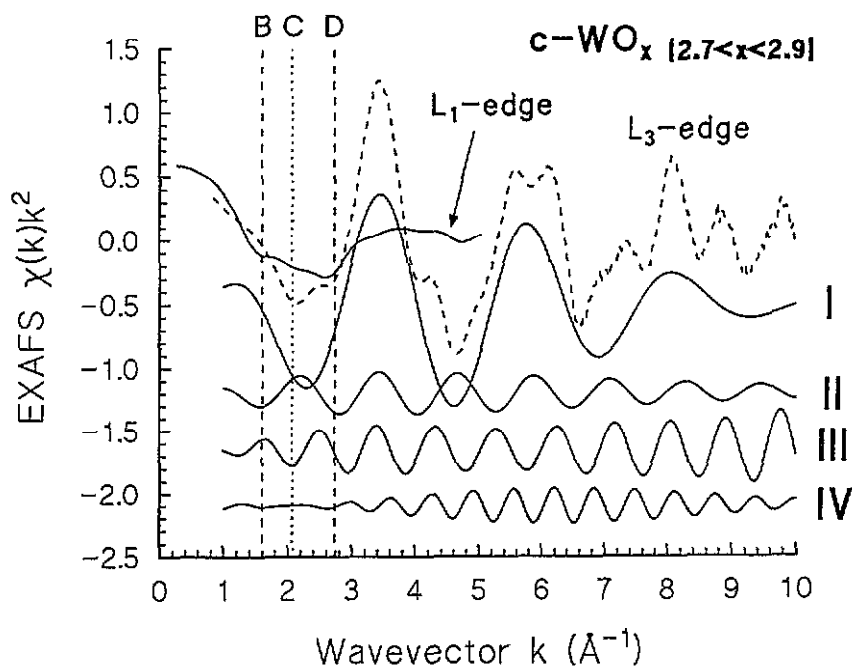


Figure 5. A comparison of the W L_1 - and L_3 -edge XAFS $\chi(k)k^2$ for $\text{WO}_{x(2.7 < x < 2.9)}$. The L_1 -edge signal was multiplied by a factor -1 , and its k scale was corrected by the difference between L_1 - and L_3 -edge phase shifts. The four contributions to the L_3 -edge XAFS, labelled in figure 3(b) and extracted by the back Fourier transform procedure, are also shown. The features B, C and D have the same meaning as in figure 4.

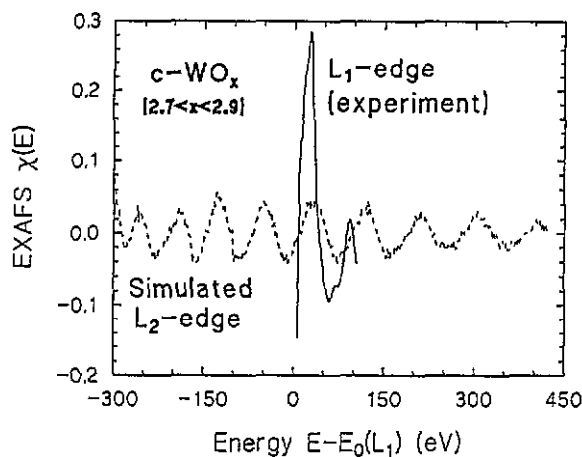


Figure 6. Experimental XAFS $\chi(E)$ of the tungsten L_1 edge in $\text{WO}_{x(2.7 < x < 2.9)}$ (full curve). The broken curve shows the contribution of the W L_2 -edge XAFS simulated from the W L_3 -edge XAFS according to (2).

shown in figure 5 was modified: the amplitude was multiplied by (-1) , and the k scale was

slightly 'squeezed' by a factor 0.96. After this correction, one can see that the fine structure of both spectra at low k -values is similar. The main shape of the L₁ signal is due to SS by oxygen atoms located in the first coordination shell. The additional fine structure appears because of the MS effects in the first shell (features B and D). The feature C is attributed to the SS and MS signals coming from tungsten atoms in the second shell. Its amplitude varies strongly in the WO_{3-x} series (see figure 4) and correlates with the amplitude of the second-shell peak in the FT (the peak III in figure 3(b)). Besides the signals considered, it was found that there is an additional contribution to the L₁-edge XAFS coming from the L₂-edge XAFS. Its intensity is proportional to the L₂-edge MS second-shell signal. A particular example of this phenomenon is shown in figure 6 for the WO_x(2.7 < x < 2.9) crystal where the second-shell MS contribution is the strongest one (see figure 3(b)). The experimental XAFS signal above the L₂ edge is limited by the presence of the L₁ edge, therefore its contribution to the L₁ XAFS region was simulated using the experimental L₃-edge XAFS extending more than 1000 eV beyond the absorption edge. Such an approach is justified if we assume that the spin of the photoelectron remains unchanged during the scattering process. In this case, the L₂ and L₃ XAFS signals will be the same since at both edges the initial and final states of the photoelectron have the same symmetry (p and d, respectively) [11]. The contribution from the L₂-edge XAFS to the L₁-edge XAFS $\chi_{L_1}(L_2)$ was simulated using the L₃-edge signal according to the expression

$$\chi_{L_1}(L_2) = \frac{(\mu_{L_3} - \mu_{L_3}^0) \mu_{L_2}^0}{\mu_{L_3}^0 \mu_{L_1}^0} \quad (2)$$

where μ_{L_n} and $\mu_{L_n}^0$ are the total and atomic, i.e. without neighbours, absorption coefficients above the L_n edge. Thus, the experimentally measured XAFS above the L₁ edge has a composite nature belonging both to the L₁ and L₂ edges and can be expressed as

$$\chi_{L_1} = (\mu_{L_1} - \mu_{L_1}^0) / \mu_{L_1}^0 + \chi_{L_1}(L_2) \quad (3)$$

where the first term corresponds to the proper L₁-edge XAFS and the second one describes the contribution from the L₂ edge. The comparison between the experimental L₁-edge XAFS and the simulated contribution from the L₂ edge is shown in figure 6. The result obtained is similar to one found by us earlier for ReO₃ [1]: the fine structure above the L₁ edge has a very significant contribution from the previous L₂ edge when a strong MS effect within the Me_a-O-Me atomic chain is present.

3. Summary and conclusions

We presented an analysis of the tungsten L-edge x-ray absorption spectra in non-stoichiometric tungsten oxides WO_{3-x} with a perovskite-like structure. It was shown that the multiple-scattering contribution (i) strongly influences the amplitude of the XAFS signal and (ii) leads to a significant mixing of the L₂- and L₁-edge signals.

A similarity of the atomic scattering amplitudes for neighbouring atoms or atoms close in the periodic table allows us to make a more general conclusion: due to a small separation of the L₂ and L₁ edges of 5d elements, a mixing of their XAFS signals will appear above the L₁ edge for elements lying in the middle of the sixth period when linear or near-linear metal-oxygen-metal chains are present in the structure of the studied compound. It seems correct that this effect can also be present for 5d elements at the beginning of the sixth period where, at the above-emphasized conditions, a mixing between the L₃ and L₂ edges can additionally occur.

Acknowledgments

The authors are grateful to Professor E Burattini (Laboratori Nazionali di Frascati) and to the staff of the PWA laboratory for the possibility of making measurements at the PWA BX-1 beam line. They wish to thank Dr P Maistrelli (Università di Trento) for help in the characterization of WO_{3-x} polycrystals.

References

- [1] Kuzmin A, Purans J, Benfatto M and Natoli C R 1993 *Phys. Rev. B* **47** 2480–6
- [2] Rehr J J, Albers R C, Natoli C R and Stern E A 1986 *Phys. Rev. B* **34** 4350–3
- [3] Schiff L I 1955 *Quantum Mechanics* 2nd edn (New York: McGraw-Hill)
- [4] Koningsberger D C and Prins R (eds) 1988 *X-Ray Absorption: Principles, Applications, Techniques of EXAFS, SEXAFS and XANES* (New York: Wiley)
- [5] Rabe P, Tolkiehn G and Werner A 1979 *J. Phys. C: Solid State Phys.* **12** 899–905
- [6] Kuzmin A 1990 *MSc Thesis* University of Latvia (in Russian)
- [7] Balerna A, Bernieri E, Burattini E, Kuzmin A and Purans J 1990 *Proc. 2nd Eur. Conf. on Progress in X-Ray Synchrotron Radiation Research* vol 25, ed A Balerna *et al* (Bologna: SIF) pp 679–82
- [8] Balerna A, Bernieri E, Burattini E, Lusic A, Kuzmin A, Purans J and Cikmach P 1991 *Nucl. Instrum. Methods A* **308** 234–9, 240–2
- [9] Loopstra B O and Boldrini P 1966 *Acta Crystallogr.* **21** 158–62
- [10] Ruiz-López M F, Loops M, Goulon J, Benfatto M and Natoli C R 1988 *Chem. Phys.* **121** 419–37
- [11] Teo B K 1986 *EXAFS: Basic Principles and Data Analysis* (Berlin: Springer)